A new atmospheric background state to diagnose local waveguidability

Christopher Polster[1] **and Volkmar Wirth**[1]

[1]Institute for Atmospheric Physics, Johannes Gutenberg University, Mainz, Germany

Key Points:

- We construct a new atmospheric background state that is local in both space and time.
- Waveguide information can be extracted from the background state potential vorticity field.
- Our scheme enables instantaneous waveguide analysis while also reproducing established waveguide patterns after long-term aggregation.

Corresponding author: Christopher Polster, cpolster@uni-mainz.de

Abstract

A new procedure to obtain a longitudinally varying and slowly evolving atmospheric background state for the analysis of Rossby waveguides is described and discussed. The procedure is a rolling zonalization scheme, redistributing Ertel potential vorticity in a moving window to separate waves from the background. Waveguides are subsequently diagnosed from the gradient of the logarithm of potential vorticity. The effectiveness of the wave-background separation, even in large-amplitude conditions, is illustrated with reanalysis data. Established climatological mean waveguide structures are recovered from the rolling-zonalized state in the limit of long-term aggregation. Two contrasting episodes of Rossby wave packet propagation demonstrate how the evolution of waveguides derived from rolling zonalization can correspond to the development of superposed wave packets. The ability of the procedure to work with snapshots of the atmosphere provides new opportunities for waveguide research.

Plain Language Summary

Rossby waves are meridional excursions of the jet stream, a strong band of wind in the extratropics. Stationary Rossby waves can cause extreme weather at the surface and travelling waves connect the weather of remote regions on the globe. Paths along which Rossby waves preferentially develop and travel are called waveguides. To detect the presence of a waveguide in atmospheric data, the waves have to be separated from their guiding atmospheric background state first. We introduce a new separation procedure for snapshots of the atmosphere that results in a slowly evolving and longitudinally varying background state. Our background state is a new source of local waveguide information, particularly in applications where no reliable information was available previously.

1 Introduction

Waveguides are paths in the atmosphere along which Rossby wave activity is preferentially ducted (Branstator, 1983; Hoskins & Ambrizzi, 1993; Chang & Yu, 1999; Martius et al., 2010; Wirth et al., 2018). The concept of a waveguide is important for understanding teleconnection patterns facilitated by Rossby waves (Hoskins & Karoly, 1981; Hsu & Lin, 1992; Branstator, 2002; Branstator & Teng, 2017), the steering of weather systems (Chang et al., 2002), the onset of atmospheric blocking (Nakamura & Huang, 2018), extreme weather (Petoukhov et al., 2013; Kornhuber et al., 2017; White et al., 2021; Rousi et al., 2022) and sub-seasonal to seasonal weather prediction (Hoskins, 2013; Davies, 2015). In this work, we focus on the horizontal propagation of Rossby waves along the extratropical jet waveguide.

Strong and narrow jet streams are known to constitute good Rossby waveguides in the atmosphere (Manola et al., 2013; Harvey et al., 2016; Wirth, 2020). In practice, jet detection schemes (e.g. Spensberger et al., 2017) and jet-associated enhanced gradients of potential vorticity (e.g. Schwierz et al., 2004; Martius et al., 2010; Röthlisberger et al., 2016) are used to extract waveguide information from atmospheric data. Waveguides are diagnosed in barotropic analysis by tracing Rossby waves as rays refracted by the stationary wavenumber field (Karoly, 1983; Hoskins & Ambrizzi, 1993; Ambrizzi et al., 1995), though concerns about the underlying assumptions of the theory have been raised since its inception (Hoskins & Karoly, 1981; Teng & Branstator, 2019; Wirth, 2020). Figure 1 illustrates the general agreement of common diagnostic fields regarding the mean climatological waveguide patterns.

The conceptual picture considers waveguides as features of a wave-free background state onto which waves are superposed. Separating waves and background in the atmosphere post factum is a challenging and not well defined problem, as the scale of both

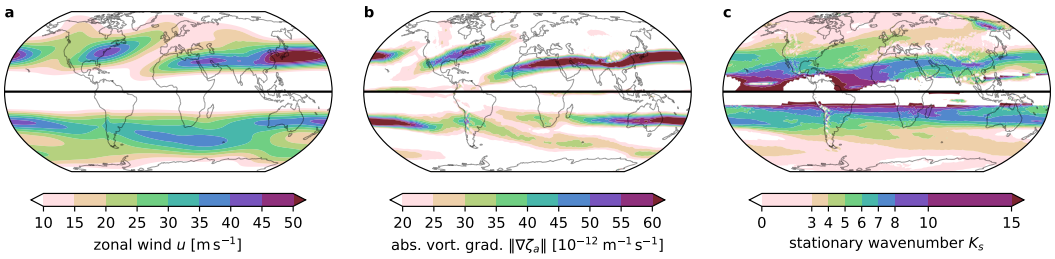

Figure 1. Barotropic waveguide diagnostic fields computed from the 1979–2022 ERA5 winter-mean horizontal wind fields on the 330 K isentrope. (a) zonal wind component u. (b) magnitude of the gradient of absolute vorticity ζ_a. (c) stationary zonal wavenumber K_s, with $K_s^2 = a\cos(\phi)^2 u^{-1}\partial_\phi\zeta_a$ (see text for symbols) and imaginary values plotted white. In general, Rossby waves are expected to propagate preferentially along maxima of these fields. Both hemispheres show winter, i.e. DJF on the northern and JJA on the southern hemisphere.

can overlap in time and space (Branstator & Teng, 2017; Wirth & Polster, 2021). Temporal and spatial filters are nevertheless often applied in practice, supported, e.g., by the finding that waveguides diagnosed from long-term means reflect the known large-scale teleconnection patterns and storm track regions (Figure 1). However, closer examination reveals representativity issues due to approximations such as zonally symmetric background states (Branstator, 1983; Borges & Sardeshmukh, 1995; Branstator, 2002; Hoskins & Ambrizzi, 1993) and internal variability (Spensberger et al., 2017) and the possibility of artifacts introduced by inadequate wave-background separation (Dritschel & Scott, 2011; Wirth & Polster, 2021). A separation scheme local in both time and space and resistant to producing artifacts in large-amplitude conditions has not been established so far.

The objective of the present work is to introduce a localized zonalization scheme as a novel method to compute a background state from a snapshot of the atmosphere for the purpose of waveguide analysis. Our scheme is both an extension and approximation of the computation of the modified Lagrangian mean state of Nakamura and Solomon (2011) and Methven and Berrisford (2015), adding longitudinal variability by means of a rolling window. Section 2 elaborates on the construction of our procedure and the used waveguide diagnostic. A background state is then computed from a reanalysis dataset (section 3) and evaluated regarding its use as a basis for waveguide analysis in section 4. We conclude with a summary and discussion in section 5.

2 Methods

2.1 Zonalization

Zonalization is a conservative rearrangement of potential vorticity (PV), such that the values of the resulting zonally symmetric PV profile are in descending order from North to South (Nakamura & Zhu, 2010). We zonalize Ertel PV, in isentropic coordinates given by $q = \frac{\zeta_a}{\sigma}$, the quotient of absolute vorticity ζ_a and isentropic density $\sigma = -\frac{1}{g}\frac{\partial p}{\partial\theta}$, with potential temperature θ, pressure p and gravitational acceleration g. The equivalent latitude ϕ_{eq} of a PV contour Q (Butchart & Remsberg, 1986; Allen & Nakamura, 2003) is implicitly defined as

$$\int_{q\geq Q} \sigma \,\mathrm{d}S = \int_{\phi\geq\phi_{\mathrm{eq}}} \sigma_{\mathrm{ref}} \,\mathrm{d}S, \tag{1}$$

where both integrals are surface integrals evaluated on an isentrope and ϕ is latitude. The background state isentropic density σ_{ref} must be prescribed for the computation.

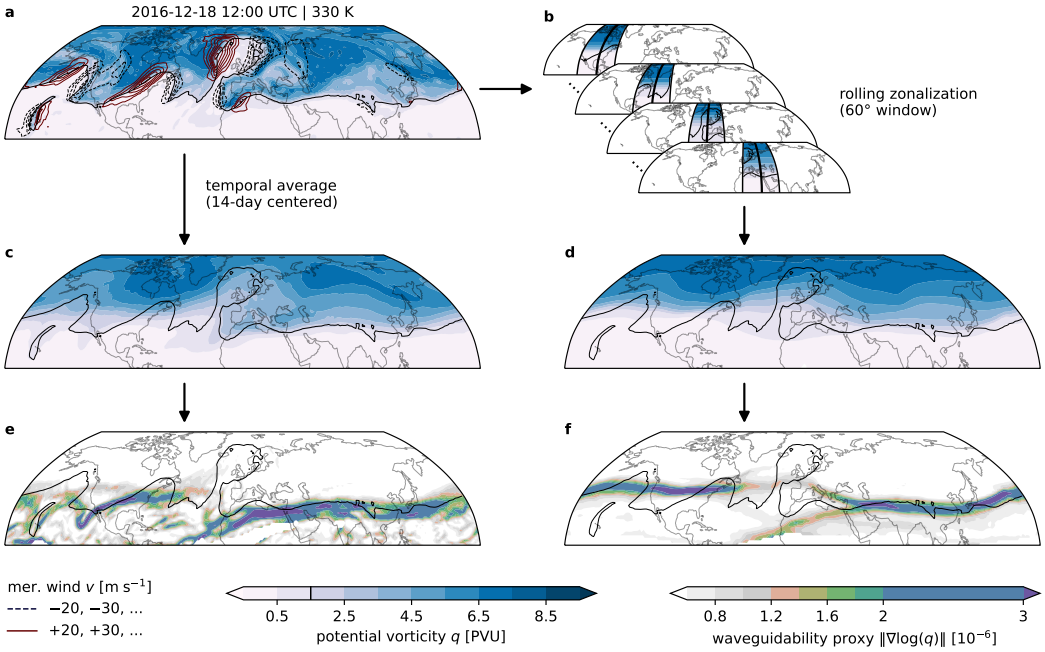

Figure 2. Comparison of time-mean and rolling-zonalized background states on the 330 K isentrope. (a) PV (filled contours) and meridional wind (red and black dashed contours) on 18 December 2016 1200 UTC. For convenience, the 1.5 PVU contour of PV is shown in all panels (solid black). (b) Rolling zonalization illustrated by four individual zonalizations for 90°W, 50°W, 10°W and 30°E. Each window's central longitude is highlighted in bold. (c) 14 day-mean PV. (d) Rolling-zonalized PV. (e,f) $\|\nabla \log(q)\|$ as a waveguide diagnostic, based on (c) and (d), respectively.

In this work, we evaluate relation (1) in a rolling fashion along longitude, using a 60°-wide window, to obtain a longitudinally varying zonalized state. The zonalized PV profile is determined for every window position based on the equivalent latitudes of a set of PV contours and assigned to the central longitude of the window (Figure 2b). We call this procedure rolling zonalization and the resulting field of zonalized PV profiles (Figure 2d) a rolling-zonalized background state.

Rolling zonalization can be adjusted to the needs of different applications by selecting different window widths, but the choice of this parameter also introduces subjectivity. For the purpose of waveguide detection, we have found results to be robust in the range of window widths from 60° to 90° and have chosen 60° as our default here. To be sure, the addition of longitudinal variation invalidates many theoretical results derived for the hemispherically zonalized state (Nakamura & Solomon, 2011; Methven & Berrisford, 2015; Ghinassi et al., 2020). We do not attempt to recover localized versions of these theorems in this work. We only note that a localized zonalized state can also change due to zonal rearrangement of PV in contrast to a hemispherically zonalized state which can exclusively change due to non-conservative processes.

The process of applying zonalization in a rolling fashion does not guarantee that PV is globally conserved, even though each individual zonalization is conservative. The loss of exact PV conservation is one of multiple approximations made to facilitate a simple and practical implementation of our procedure. A significant departure from the ELIPVI zonalization scheme of Methven and Berrisford (2015) is the omission of PV inversion

and an iteration to a consistent background isentropic density field. Instead, we prescribe σ_{ref} based on a longitudinally rolling mean of σ using the same window width as the zonalization. The lack of PV inversion also means that other "byproducts" like the background state wind are not computed in our approximation. A three-dimensional hemispheric PV inversion required for a localized ELIPVI implementation presents a significant technical challenge. For practical reasons and accessibility we do not want to incur the substantial computational costs of an inversion-based procedure. By contrast, a rolling zonalization can be computed in about 100 ms on a single CPU core.

2.2 Waveguide Diagnostic

We diagnose waveguidability, a non-binary assessment of the propensity of the atmosphere to duct Rossby waves (Manola et al., 2013; Wirth, 2020), based on the gradient of the logarithm of the background state PV obtained from the rolling zonalization. An example of this field is shown in Figure 2f. To first order, $\|\nabla \log(q)\|$ is proportional to the curvature of the flow $\nabla^2 u$ and thus related to the dispersion relation of Rossby waves (Martius et al., 2010; Bukenberger et al., 2023). We aim to avoid issues associated with strong variations of stratification when deriving the location of waveguides from $\|\nabla \log(q)\|$ (Bukenberger et al., 2023) with the rolling mean-smoothed σ_{ref}. Regions where $|q| < 0.1\,\mathrm{PVU}$ ($1\,\mathrm{PVU} = 10^{-6}\,\mathrm{K\,m^2\,kg^{-1}\,s^{-1}}$) are excluded in our waveguide analysis to avoid the divergence of the logarithm when $q \to 0$. As a simple criterion for the presence of a waveguide, we require $\|\nabla \log(|q|)\| > 1.2 \times 10^{-6}$, with q in PVU. We have verified that our results are not sensitive to the choice of this threshold.

3 Data

We process ERA5 (Hersbach et al., 2020, 2023) reanalysis fields of u, v and T from 1979 to 2022 (6-hourly). The input fields are obtained with 1.5° horizontal resolution on 18 pressure levels (50 to 850 hPa in steps of 50 hPa; 70 hPa additionally). We compute potential temperature and isentropic density on pressure levels, then interpolate to isentropes. Vorticity is computed from the interpolated winds and combined with the interpolated isentropic density to calculate PV. Surface integrals for the zonalization are evaluated with a conditional boxcounting quadrature scheme with regions outside the input data range omitted. We zonalize each hemisphere separately.

4 Results

4.1 A First Look

We take a first look at a rolling-zonalized state in Figure 2d. The selected date is from a European blocking event in December 2016 (Maddison et al., 2019; Polster & Wirth, 2023). The rolling-zonalized PV exhibits a wavenumber 2 to 3 pattern in the midlatitudes. The meridional spacing of background state PV contours widens locally over western Europe and resembles an often assumed background state configuration of scale interaction models of atmospheric blocking (Luo et al., 2023). The associated weakened gradient of PV is reflected in our waveguide diagnostic field (Figure 2f). With a threshold of $1.2{\times}10^{-6}$, we detect an interruption of the waveguide in the blocking region, while a strong and continuous waveguide is found over subtropical Asia and the midlatitude Pacific and North American regions. Interestingly, our scheme detects strong waveguidability over Asia despite no wave being present there.

Comparing the rolling-zonalized (Figure 2d) and the 14-day temporally averaged PV fields (Figure 2c), we find some common features but also important differences in the details. Generally, magnitudes of log-PV gradients are similar and the interruption of the waveguide at the blocking is found in both background states. The temporally averaged PV is also dominated by a wavenumber 2 to 3 structure. However, meridional

PV profiles in the temporally averaged field are non-monotonic and contour overturning at the block location indicates a failure of the temporal average to remove a stationary, large-amplitude eddy. A higher degree of small scale structure in the temporally averaged state translates to considerably noisier waveguides in the associated $\|\nabla \log(q)\|$ field (Figure 2e). The remains of synoptic-scale troughs are visible over the North Pacific and the Asian subtropical waveguide starts further west without a connecting arm from western Europe. In the rolling-zonalized state, the latitude of the waveguide over North America corresponds better to the central latitude of the superposed wave packet than in the time-averaged state.

4.2 Filtering Properties

The temporal evolution of a hemispherically zonalized state is known to be inherently slow (Nakamura & Solomon, 2011; Methven & Berrisford, 2015). Figure 2 suggests that rolling zonalization can produce fields with a broadly similar structure compared to those produced by a temporal filter, despite only using instantaneous data. In an analysis of 44 years of 6-hourly rolling-zonalized PV based on autocorrelation and spectral decomposition we found that the rolling-zonalized background state also evolves inherently slowly, although the characteristics of the temporal behaviour do not correspond directly to that of any simple temporal filter we compared against (not shown).

A rolling-zonalized state (60˚ window) cuts off virtually all contributions of waves with wavenumbers equal to or larger than 5 in the zonal wavenumber power spectrum of PV (Figure 3a). Wavenumbers 1, 2 and 3 contribute almost all spectral power in the Northern Hemisphere midlatitudes, with only minor contributions from wavenumber 4. We consider the rolling-zonalized state state therefore to be free of synoptic- and smaller-scale eddies. Widening the window of the rolling zonalization to 90˚ reduces the power in wavenumbers 2 to 4 significantly and moves the cut-off wavelength to $k = 4$. By comparison, a 14-day rolling mean still has as much power in wavenumber 6 than the 60˚ rolling-zonalized state in wavenumber 4 and correlates more strongly with the spectrum of the original PV. In the spectral comparison of Figure 3a, the 60˚ rolling-zonalized state is closest to the climatological mean state. Similar to the temporal filtering, the spatial filtering properties of rolling zonalization are generally not unlike, but in details importantly different to those of simple averaging procedures.

4.3 Climatological Waveguide Occurrence

Using the 1.2×10^{-6} threshold, we compute the gridpoint-wise occurrence frequency of waveguides in the rolling-zonalized state. Figure 3b shows the winter-time waveguide occurrence for our default window with of 60˚ longitude on 330 K. Frequent occurrence of an Asian subtropical waveguide extending into the Pacific and a North American/North Atlantic waveguide can be identified on the Northern Hemisphere. On the Southern Hemisphere, a band of more than 40% waveguide occurence extends around the globe in the midlatitudes with waveguides occurring preferentially in the Pacific sector from Australia to South America. Figure 3c shows the same analysis for a 90˚-wide window, resulting in more zonally elongated waveguide occurrence features. The identity of the North Atlantic waveguide as a feature separate from the North Pacific waveguide is less pronounced but differences between the window widths are otherwise small.

We compare the climatological mean barotropic waveguide diagnostic fields in Figure 1 with the waveguide occurrence frequency field in Figure 3b. The climatological mean winter waveguide structure is broadly reproduced in the long-term aggregated waveguide information from individual snapshots of the rolling-zonalized atmosphere. Relative signal strengths of co-located features in Figure 1 and Figure 3b are similar. However, the waveguide signal associated with the North Atlantic jet does not extend as far towards Europe in the frequency field of the rolling-zonalized state and a secondary waveg-

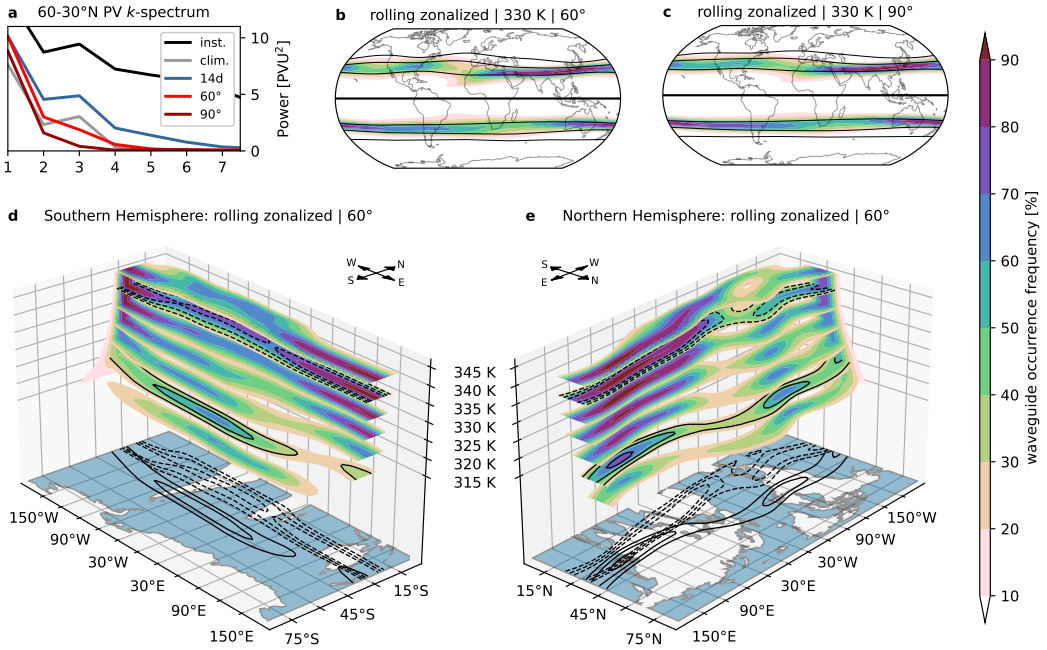

Figure 3. (a) Zonal Wavenumber spectra of instantaneous PV (black), climatological-mean PV (gray), 14 day-rolling-averaged PV (blue) and 60°- (light red) and 90°-window (dard red) rolling-zonalized PV. All spectra of winter months only, spectral power averaged from 60 to 30°N on 330 K. (b,c) Climatological waveguide occurrence on 330 K during winter, derived from a rolling-zonalized state with a 1.2×10^{-6} waveguide detection threshold. Mean contours of rolling-zonalized PV are shown in black. Comparison of 60° (b) and 90° (c) window widths. (d,e) Waveguide occurrence as in (b) but for isentropic levels from 315 to 345 K in steps of 5 K in a 3D visualization for each hemisphere. Selected contours from the 320 (solid) and 340 K (dashed) isentropic levels are reproduced on the bottom maps for orientation. Note that the actual surface of the planet is not a surface of constant potential temperature as depicted here.

uide over the Atlantic and Indian Ocean on the Southern Hemisphere is missing. Differences in the waveguide features can be contextualized with the vertical structure of waveguide occurrence in Figure 3d and e. The vertical structure shows the distinct identities of the North Atlantic and Asian/Pacific waveguides on the Northern Hemisphere more clearly than 330 K alone. The midlatitude waveguides over the North and South Atlantic oceans are primarily found on lower isentropic levels than 330 K, while the subtropical waveguides are found at higher levels (Martius et al., 2010; Martin, 2021).

4.4 Two Contrasting Episodes

We use a refined Hovmöller diagram (Martius et al., 2006) to further illuminate the waveguide evolution around the December 2016 blocking episode introduced in section 4.1 and Figure 2. Note that the generation of such contour-following Hovmöller diagrams is particularly easy in the rolling-zonalized state as each PV contour intersects a meridian at most once by construction. Figure 4c shows the evolution of $\|\nabla \log(q)\|$, our waveguidability metric, along the 1.5 PVU contour on 330 K for the 2016 episode. In the snapshot for 15 December (Figure 4b), a Rossby wave packet (RWP) stretches from North America across the North Atlantic into northern Europe, superposed onto a strong waveguide over North America. The waveguide is weaker over the Atlantic with a connection

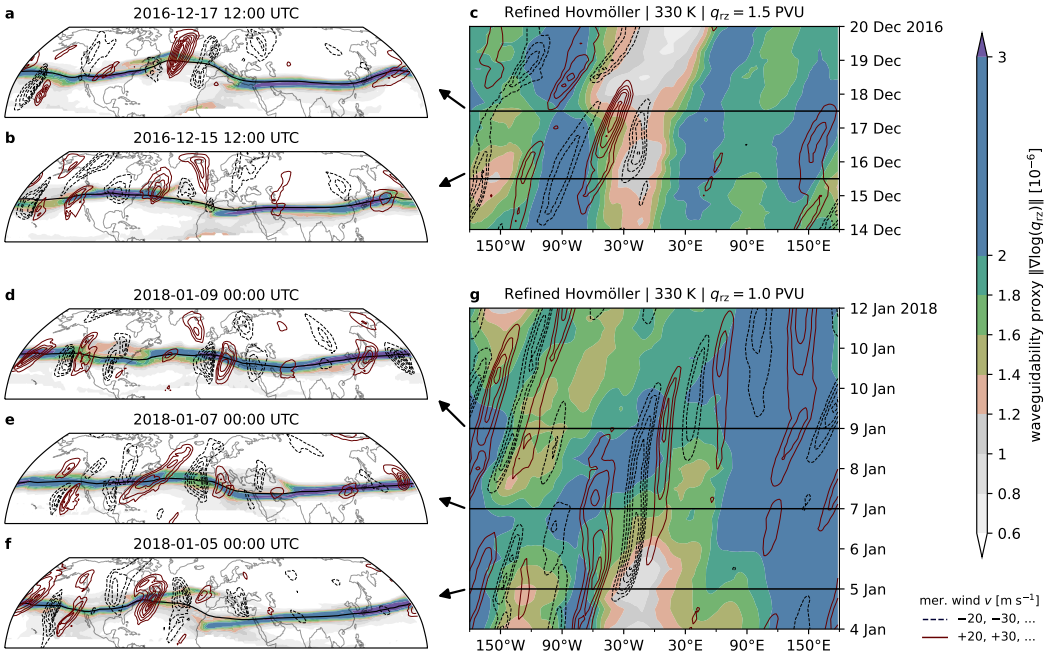

Figure 4. (a,b) $\|\nabla \log(q)\|$ waveguidability diagnostic (filled contours), 1.5 PVU contour of rolling-zonalized PV (black) and meridional wind (dark red/blue contours, in steps of 10 m s^{-1} starting from ±20 m s^{-1}) on 330 K for 17 and 15 December 2016 1200 UTC, respectively. (c) refined Hovmöller diagram of the grad-log-PV waveguide diagnostic (filled contours) and meridional wind (contours). Data is extracted with a 7.5° boxcar smoothing kernel along the contour of 1.5 PVU. (d,e,f) Like (a) but for 9, 7 and 5 December 2018, respectively, and with a PV contour of 1 PVU. (g) Like (c) but for 4 to 12 December 2018 and 1 PVU.

to the subtropical waveguide over Asia and a second short branch pointing towards northern Europe. Over the next two days the waveguide strengthens over the Atlantic while shifting northward together with the 1.5 PVU contour (Figure 4a). A day later, the waveguide is interrupted (c.f. Figure 2f) and the propagation of the RWP ceases as the block has been established (Polster & Wirth, 2023), with low waveguidability dominating the sector after 17 December (Figure 4c).

A different evolution of waveguide and wave is seen in an episode from January 2018 (Figure 4d–g). On 5 January (Figure 4f), a North Atlantic waveguide ends about 20° further north than a subtropical waveguide over Africa starts, with no significant connection between both. A Rossby wave packet stretches across the Atlantic along the waveguide. Strong meridional winds develop over the North Atlantic but the wave packet does not propagate through the African/European region at first. During 6 January, the two waveguides connect over the Mediterranean (Figure 4e,g) and a wave signal emerges in the subtropics at the same time. By 9 January, a strong waveguide has been established from the North Atlantic across Asia to the North Pacific (Figure 4d). The evolution of the wave packet appears to occur along this waveguide, with new meridional wind extrema developing over the Arabian peninsula and further downstream in the following days (Figure 4g).

The two episodes exhibit opposite RWP propagation characteristics in the African/European region. While the incoming RWP in December 2016 develops into a block with no downstream development over Asia, the wave packet in January 2018 continues development

along the subtropical waveguide (akin to the equatorward wave energy transfer described by Martius et al., 2010). The parallel evolutions of the midlatitude and subtropical waveguides in these two episodes reflect these (non-)propagation patterns: the waveguides are effectively disconnected during the 2016 episode, while the waveguides connect in 2018.

5 Summary and Discussion

We have introduced a new procedure, rolling zonalization, to compute a three-dimensional background state of the atmosphere that evolves with time. The procedure consists of a rearrangement of potential vorticity in a longitudinally rolling sector on a hemisphere, based on the concept of equivalent latitude. Rolling zonalization combines aspects of both a spatial and a temporal filter. Synoptic-scale eddies of arbitrary amplitude are eliminated effectively by the zonalization. The resulting background state is slowly evolving even though no information other than the instantaneous state of the atmosphere is required to compute it.

Localizing zonalization with a rolling window is straightforward, but it is only an approximation of a scheme consistent with the underlying formalism. We do not compute consistent background fields of isentropic density or wind and strict PV conservation is not guaranteed, although we have observed good PV conservation for our setup. We leave the formulation of a theory of wave-mean flow interaction that accomodates our localized zonalized background state to future work. Our present objective is to advance the state of practical application.

Using the log-PV gradient of the rolling-zonalized background state as a waveguide diagnostic, we were able to recover the established structure of the winter-time climatological waveguides in the extratropics. The aggregation of instantaneous waveguide information into a frequency-based perspective on waveguide occurrence complements earlier climatological mean-based results (see also White, 2019). Two contrasting episodes of Rossby wave packet propagation demonstrated how the zonalization-derived waveguides can correspond to the local development of superposed wave trains. An interrupted waveguide in the first episode coincided with the onset of a block. A connected waveguide in the second episode coincided with a transfer of wave activity from the midlatitude to the subtropical waveguide.

We can envisage further fine tuning of the rolling zonalization procedure and waveguide diagnostics. Instead of a threshold-based binary view of waveguide occurrence, more nuanced information on waveguidabililty should be extractable from the background state. Local wave activity (Huang & Nakamura, 2016, 2017; Ghinassi et al., 2018), computed with respect to the longitudinally varying zonalized background state, presents a more consistent measure of local waviness than the meridional wind. We intend to explore the relationship between waveguidability properties of the rolling-zonalized background state and wave packet propagation further in the future.

An atmospheric background state which is local in time and space and which is computable from instantaneous data enables diagnostics to be applied in the full range of lead times in forecast applications. Individual events can be investigated with regard to the influence of teleconnection patterns or the potential of resonance along a circumglobal waveguide. These are new and sought-after possibilities for current waveguidability research (e.g. White et al., 2021; Riboldi et al., 2022).

Open Research

The code to reproduce the data analysis and all figures of this article is preserved online (Polster, 2023). Procedures to compute the rolling zonalization are provided in a Python package included in the associated code repository. ERA5 data (Hersbach et

al., 2023) was downloaded from the Copernicus Climate Change Service (C3S) Climate Data Store. The results contain modified Copernicus Climate Change Service information 2023. Neither the European Commission nor ECMWF is responsible for any use that may be made of the Copernicus information or data it contains.

Acknowledgments

We thank M. Riemer for valuable discussions about the rolling zonalization and its applications. The research leading to these results has been done within the Transregional Collaborative Research Center SFB/TRR 165 "Waves to Weather" funded by the German Science Foundation (DFG).

References

Allen, D. R., & Nakamura, N. (2003). Tracer Equivalent Latitude: A Diagnostic Tool for Isentropic Transport Studies. *Journal of the Atmospheric Sciences*, *60*(2), 287–304. doi: 10.1175/1520-0469(2003)060⟨0287:TELADT⟩2.0.CO;2

Ambrizzi, T., Hoskins, B. J., & Hsu, H.-H. (1995). Rossby Wave Propagation and Teleconnection Patterns in the Austral Winter. *Journal of the Atmospheric Sciences*, *52*(21), 3661–3672. doi: 10.1175/1520-0469(1995)052⟨3661:RWPATP⟩2.0.CO;2

Borges, M. D., & Sardeshmukh, P. D. (1995). Barotropic Rossby Wave Dynamics of Zonally Varying Upper-Level Flows during Northern Winter. *Journal of the Atmospheric Sciences*, *52*(21), 3779–3796. doi: 10.1175/1520-0469(1995)052⟨3779:BRWDOZ⟩2.0.CO;2

Branstator, G. (1983). Horizontal Energy propagation in a Barotropic Atmosphere with Meridional and Zonal Structure. *Journal of Atmospheric Sciences*, *40*(7), 1689 – 1708. (Place: Boston MA, USA Publisher: American Meteorological Society) doi: 10.1175/1520-0469(1983)040⟨1689:HEPIAB⟩2.0.CO;2

Branstator, G. (2002, July). Circumglobal Teleconnections, the Jet Stream Waveguide, and the North Atlantic Oscillation. *Journal of Climate*, *15*(14), 1893–1910. (Publisher: American Meteorological Society) doi: 10.1175/1520-0442(2002)015⟨1893:CTTJSW⟩2.0.CO;2

Branstator, G., & Teng, H. (2017). Tropospheric Waveguide Teleconnections and Their Seasonality. *Journal of the Atmospheric Sciences*, *74*(5), 1513–1532. doi: 10.1175/JAS-D-16-0305.1

Bukenberger, M., Rüdisühli, S., & Schemm, S. (2023). Jet stream dynamics from a PV gradient perspective: The method and its application to a km-scale simulation. *Quarterly Journal of the Royal Meteorological Society*, qj.4513. doi: 10.1002/qj.4513

Butchart, N., & Remsberg, E. E. (1986). The Area of the Stratospheric Polar Vortex as a Diagnostic for Tracer Transport on an Isentropic Surface. *Journal of Atmospheric Sciences*, *43*(13), 1319–1339. doi: 10.1175/1520-0469(1986)043⟨1319:TAOTSP⟩2.0.CO;2

Chang, E. K. M., Lee, S., & Swanson, K. L. (2002). Storm Track Dynamics. *Journal of Climate*, *15*(16), 2163 – 2183. doi: 10.1175/1520-0442(2002)015⟨02163:STD⟩2.0.CO;2

Chang, E. K. M., & Yu, D. B. (1999). Characteristics of Wave Packets in the Upper Troposphere. Part I: Northern Hemisphere Winter. *Journal of the Atmospheric Sciences*, *56*(11), 1708–1728. doi: 10.1175/1520-0469(1999)056⟨1708:COWPIT⟩2.0.CO;2

Davies, H. C. (2015). Weather chains during the 2013/2014 winter and their significance for seasonal prediction. *Nature Geoscience*, *8*(11), 833–837. doi: 10.1038/ngeo2561

Dritschel, D. G., & Scott, R. K. (2011). Jet sharpening by turbulent mixing. *Philo-*

sophical Transactions of the Royal Society A: Mathematical, Physical and Engineering Sciences, *369*(1937), 754–770. doi: 10.1098/rsta.2010.0306

Ghinassi, P., Baumgart, M., Teubler, F., Riemer, M., & Wirth, V. (2020). A Budget Equation for the Amplitude of Rossby Wave Packets Based on Finite-Amplitude Local Wave Activity. *Journal of the Atmospheric Sciences*, *77*(1), 277–296. doi: 10.1175/JAS-D-19-0149.1

Ghinassi, P., Fragkoulidis, G., & Wirth, V. (2018). Local Finite-Amplitude Wave Activity as a Diagnostic for Rossby Wave Packets. *Monthly Weather Review*, *146*(12), 4099–4114. doi: 10.1175/MWR-D-18-0068.1

Harvey, B. J., Methven, J., & Ambaum, M. H. P. (2016). Rossby wave propagation on potential vorticity fronts with finite width. *Journal of Fluid Mechanics*, *794*, 775–797. doi: 10.1017/jfm.2016.180

Hersbach, H., Bell, B., Berrisford, P., Biavati, G., Horányi, A., Muñoz Sabater, J., ... others (2023). *ERA5 hourly data on pressure levels from 1940 to present.* Copernicus Climate Change Service (C3S) Climate Data Store (CDS). doi: 10.24381/cds.bd0915c6

Hersbach, H., Bell, B., Berrisford, P., Hirahara, S., Horányi, A., Muñoz-Sabater, J., ... Thépaut, J. (2020). The ERA5 global reanalysis. *Quarterly Journal of the Royal Meteorological Society*, *146*(730), 1999–2049. doi: 10.1002/qj.3803

Hoskins, B. J. (2013). The potential for skill across the range of the seamless weather-climate prediction problem: a stimulus for our science. *Quarterly Journal of the Royal Meteorological Society*, *139*(672), 573–584. doi: 10.1002/qj.1991

Hoskins, B. J., & Ambrizzi, T. (1993, June). Rossby Wave Propagation on a Realistic Longitudinally Varying Flow. *Journal of the Atmospheric Sciences*, *50*(12), 1661–1671. (Publisher: American Meteorological Society) doi: 10.1175/1520-0469(1993)050⟨1661:RWPOAR⟩2.0.CO;2

Hoskins, B. J., & Karoly, D. J. (1981). The Steady Linear Response of a Spherical Atmosphere to Thermal and Orographic Forcing. *Journal of the Atmospheric Sciences*, *38*(6), 1179–1196. doi: 10.1175/1520-0469(1981)038⟨1179:TSLROA⟩2.0.CO;2

Hsu, H.-H., & Lin, S.-H. (1992). Global Teleconnections in the 250-mb Streamfunction Field during the Northern Hemisphere Winter. *Monthly Weather Review*, *120*(7), 1169–1190. doi: 10.1175/1520-0493(1992)120⟨1169:GTITMS⟩2.0.CO;2

Huang, C. S. Y., & Nakamura, N. (2016). Local Finite-Amplitude Wave Activity as a Diagnostic of Anomalous Weather Events. *Journal of the Atmospheric Sciences*, *73*(1), 211–229. doi: 10.1175/JAS-D-15-0194.1

Huang, C. S. Y., & Nakamura, N. (2017). Local wave activity budgets of the wintertime Northern Hemisphere: Implication for the Pacific and Atlantic storm tracks. *Geophysical Research Letters*, *44*(11), 5673–5682. doi: 10.1002/2017GL073760

Karoly, D. J. (1983, March). Rossby wave propagation in a barotropic atmosphere. *Dynamics of Atmospheres and Oceans*, *7*(2), 111–125. doi: 10.1016/0377-0265(83)90013-1

Kornhuber, K., Petoukhov, V., Petri, S., Rahmstorf, S., & Coumou, D. (2017). Evidence for wave resonance as a key mechanism for generating high-amplitude quasi-stationary waves in boreal summer. *Climate Dynamics*, *49*(5-6), 1961–1979. doi: 10.1007/s00382-016-3399-6

Luo, D., Luo, B., & Zhang, W. (2023). A Perspective on the Evolution of Atmospheric Blocking Theories: From Eddy-Mean flow Interaction to Nonlinear Multiscale Interaction. *Advances in Atmospheric Sciences*. doi: 10.1007/s00376-022-2194-z

Maddison, J. W., Gray, S. L., Martínez-Alvarado, O., & Williams, K. D. (2019). Upstream Cyclone Influence on the Predictability of Block Onsets over the Euro-Atlantic Region. *Monthly Weather Review*, *147*(4), 1277–1296. doi:

10.1175/MWR-D-18-0226.1

Manola, I., Selten, F., de Vries, H., & Hazeleger, W. (2013, September). "Waveguidability" of idealized jets. *Journal of Geophysical Research: Atmospheres*, *118*(18), 10,432–10,440. doi: 10.1002/jgrd.50758

Martin, J. E. (2021). Recent Trends in the Waviness of the Northern Hemisphere Wintertime Polar and Subtropical Jets. *Journal of Geophysical Research: Atmospheres*, *126*(9). doi: 10.1029/2020JD033668

Martius, O., Schwierz, C., & Davies, H. C. (2006, January). A refined Hovmöller diagram. *Tellus A: Dynamic Meteorology and Oceanography*, *58*(2), 221–226. doi: 10.1111/j.1600-0870.2006.00172.x

Martius, O., Schwierz, C., & Davies, H. C. (2010, March). Tropopause-Level Waveguides. *Journal of the Atmospheric Sciences*, *67*(3), 866–879. doi: 10.1175/2009JAS2995.1

Methven, J., & Berrisford, P. (2015). The slowly evolving background state of the atmosphere. *Quarterly Journal of the Royal Meteorological Society*, *141*(691), 2237–2258. doi: 10.1002/qj.2518

Nakamura, N., & Huang, C. S. Y. (2018). Atmospheric blocking as a traffic jam in the jet stream. *Science*, *361*(6397), 42–47. doi: 10.1126/science.aat0721

Nakamura, N., & Solomon, A. (2011). Finite-Amplitude Wave Activity and Mean Flow Adjustments in the Atmospheric General Circulation. Part II: Analysis in the Isentropic Coordinate. *Journal of the Atmospheric Sciences*, *68*(11), 2783–2799. doi: 10.1175/2011JAS3685.1

Nakamura, N., & Zhu, D. (2010). Finite-Amplitude Wave Activity and Diffusive Flux of Potential Vorticity in Eddy–Mean Flow Interaction. *Journal of the Atmospheric Sciences*, *67*(9), 2701–2716. doi: 10.1175/2010JAS3432.1

Petoukhov, V., Rahmstorf, S., Petri, S., & Schellnhuber, H. J. (2013). Quasiresonant amplification of planetary waves and recent Northern Hemisphere weather extremes. *Proceedings of the National Academy of Sciences*, *110*(14), 5336–5341. doi: 10.1073/pnas.1222000110

Polster, C. (2023). *wavestoweather/Rolling-Zonalization: v1.0.* Zenodo. Retrieved 2023-08-28, from `https://doi.org/10.5281/zenodo.8300732` doi: 10.5281/zenodo.8300732

Polster, C., & Wirth, V. (2023). The Onset of a Blocking Event as a "Traffic Jam": Characterization with Ensemble Sensitivity Analysis. *Journal of the Atmospheric Sciences*, *80*(7), 1681–1699. doi: 10.1175/JAS-D-21-0312.1

Riboldi, J., Rousi, E., D'Andrea, F., Rivière, G., & Lott, F. (2022). Circumglobal Rossby wave patterns during boreal winter highlighted by space–time spectral analysis. *Weather and Climate Dynamics*, *3*(2), 449–469. doi: 10.5194/wcd-3-449-2022

Rousi, E., Kornhuber, K., Beobide-Arsuaga, G., Luo, F., & Coumou, D. (2022). Accelerated western European heatwave trends linked to more-persistent double jets over Eurasia. *Nature Communications*, *13*(1), 3851. doi: 10.1038/s41467-022-31432-y

Röthlisberger, M., Martius, O., & Wernli, H. (2016, January). An algorithm for identifying the initiation of synoptic-scale Rossby waves on potential vorticity waveguides: Initiation of Rossby Waves on PV Waveguides. *Quarterly Journal of the Royal Meteorological Society*, *142*(695), 889–900. doi: 10.1002/qj.2690

Schwierz, C., Dirren, S., & Davies, H. C. (2004). Forced Waves on a Zonally Aligned Jet Stream. *Journal of the Atmospheric Sciences*, *61*(1), 73–87. doi: 10.1175/1520-0469(2004)061⟨0073:FWOAZA⟩2.0.CO;2

Spensberger, C., Spengler, T., & Li, C. (2017). Upper-Tropospheric Jet Axis Detection and Application to the Boreal Winter 2013/14. *Monthly Weather Review*, *145*(6), 2363–2374. doi: 10.1175/MWR-D-16-0467.1

Teng, H., & Branstator, G. (2019, December). Amplification of Waveguide Teleconnections in the Boreal Summer. *Current Climate Change Reports*, *5*(4), 421–

458 432. doi: 10.1007/s40641-019-00150-x
459 White, R. H. (2019). Detecting waveguides for atmospheric planetary waves: con-
460 nections to extreme weather events. In C. Chen, A. Charantonis, J. Runge,
461 & J. Brajard (Eds.), *Proceedings of the 9th International Workshop on Cli-*
462 *mate Informatics: CI2019 9 (No. NCAR/TN- 561+PROC)* (pp. 219–223).
463 UCAR/NCAR. doi: 10.5065/Y82J-F154
464 White, R. H., Kornhuber, K., Martius, O., & Wirth, V. (2021, November). From
465 Atmospheric Waves to Heatwaves: A Waveguide Perspective for Under-
466 standing and Predicting Concurrent, Persistent and Extreme Extratropi-
467 cal Weather. *Bulletin of the American Meteorological Society*, 1–35. doi:
468 10.1175/BAMS-D-21-0170.1
469 Wirth, V. (2020, April). Waveguidability of idealized midlatitude jets and the lim-
470 itations of ray tracing theory. *Weather and Climate Dynamics*, *1*(1), 111–125.
471 doi: 10.5194/wcd-1-111-2020
472 Wirth, V., & Polster, C. (2021, July). The Problem of Diagnosing Jet Waveguid-
473 ability in the Presence of Large-Amplitude Eddies. *Journal of the Atmospheric*
474 *Sciences*. doi: 10.1175/JAS-D-20-0292.1
475 Wirth, V., Riemer, M., Chang, E. K. M., & Martius, O. (2018). Rossby Wave
476 Packets on the Midlatitude Waveguide—A Review. *Monthly Weather Review*,
477 *146*(7), 1965–2001. doi: 10.1175/MWR-D-16-0483.1